Spatial Time-Dependent Reliability Analysis of Reinforced Concrete Slab Bridges Subject to Realistic Traffic Loading

Donya Hajializadeh[1], Mark G. Stewart[2], Bernard Enright[3], Eugene OBrien[4,1]

[1]Roughan & O'Donovan Innovative Solutions, Ireland
[2]The University of Newcastle, Australia
[3]Dublin Institute of Technology, Ireland
[4]University College Dublin, Ireland

1 Abstract

Resistance and loads are often correlated in time and space. The paper assesses the influence of these correlations on structural reliability/probability of failure for a typical two-lane RC slab bridge under realistic traffic loading. Spatial variables for structural resistance are cover and concrete compressive strength, which in turn affect the strength and chloride-induced corrosion of RC elements. Random variables include pit depth and model error. Correlation of weights between trucks in adjacent lanes and inter-vehicle gaps are also included and are calibrated against Weigh-In-Motion (WIM) data. Reliability analysis of deteriorating bridges needs to incorporate uncertainties associated with parameters governing the deterioration process and loading. One of the major unanswered questions in the work carried out to date is the influence of spatial variability of load and resistance on failure probability. Spatial variability research carried out to date has been mainly focused on predicting the remaining lifetime of a corroding structure and spatial variability of material, dimensional and environmental properties. A major shortcoming in the work carried out to date is the lack of an allowance for the spatial variability of applied traffic loads. In this paper, a 2-dimensional (2D) random field is developed where load effects and time-dependent structural resistance are calculated for each segment in the field. The 2D spatial time-dependent reliability analysis of an RC slab bridge found that a spatially correlated resistance results in only a small increase in probability of failure. Despite the fact that load effect at points along the length of a bridge are strongly correlated, the combined influence of correlation in load and resistance on probability of failure is small.

2 Introduction

The timing and extent of infrastructure maintenance actions is an important consideration for asset owners, particularly in relation to deteriorating bridges and increasing traffic volumes and loadings. While the costs of inspection, maintenance and repair increase (Stewart and Rosowsky 1998; Costa and Appleton 1999; Frangopol et al. 2001), budgets are being curtailed due to adverse social and economic circumstances experienced in many countries. Maintenance costs now constitute a substantial portion of the national highways budget in many developed countries (O'Connor and Kenshel 2012). The annual expenditure on maintenance and repair on national bridges in England is in the order of €180 million, in France is about €50 million, in Norway €30 million and in the Netherlands about €100 million (Li 2004). With such great expenditures, any realized efficiency or optimization in bridge asset management can deliver substantial savings. To optimize and manage the available budget for repair and maintenance, there is a need for rational decision making methods and more accurate methods of safety assessment. Reliability- or failure probability-based decision making is a powerful methodology for such optimization.

In recent times, probabilistic and reliability-based approaches have been widely used to quantify bridge safety (Val and Melchers 1997; Val et al. 2000; Vu and Stewart 2000; Akgül and Frangopol 2004b; O'Connor and Enevoldsen 2007; Marsh and Frangopol 2008; O'Connor et al. 2009; O'Connor and Enevoldsen 2009). Reliability analysis of deteriorating bridges needs to incorporate uncertainties associated with parameters governing the deterioration process and loading. One of the major unanswered questions in the work carried out to date is the influence of spatial variability of load and resistance on structural reliability.

Concrete material properties, dimensions and environmental parameters will vary spatially over a structure due to a number of factors including material variations and workmanship. For example, Fazio et al. (1999) found significant spatial variability in chloride content, concrete cover, concrete strength and corrosion damage in a 39 year old bridge deck. Variation in material properties, loading, structural dimensions and environmental exposure conditions can lead to spatially variable deterioration and may be included in predictive strength models to achieve more realistic results. The advantage of incorporating spatial variability into stochastic models has been demonstrated in studies on the prediction of likelihood and extent of corrosion damage in Reinforced Concrete (RC) structures (Sterritt et al. 2001; Li et al. 2004; Malioka and Faber 2004; Sudret et al. 2006; Stewart and Mullard 2007).

Engelund and Sørensen (1998) consider spatial uncertainties associated with the critical threshold for initiation of corrosion of reinforcement, chloride diffusion coefficient, and surface chloride concentration. First-Order Reliability Method (FORM) and Second-Order Reliability Method (SORM) analyses are applied to estimate distributions for time to initiation of corrosion. Stewart (2004) discretised an RC beam into a series of segments to find the spatial variability of pitting corrosion in RC beams. He generates maximum pit depths for each reinforcing steel bar in a one-dimensional (1D) random field to assess the effect of spatial variability on structure reliability.

A 2D time-dependent reliability model allowing for spatial variability is developed by Vu and Stewart (2005), where concrete properties, concrete cover and the surface chloride concentrations are treated as random fields. Malioka and Faber (2004) suggest that corrosion initiation and propagation are spatially variable due to the variability in concrete batches and workmanship during construction of RC structures. A random field approach is then presented to model the spatial variability of concrete permeability and is used within a reliability analysis to predict the percentage of a structure that exhibits degradation at a specified point in time.

A spatial time-dependent reliability analysis, considering shear and flexure limit states, is developed by Stewart (2009), using improved probabilistic models of pitting corrosion (Stewart and Al-Harthy 2008). He incorporates ductile and brittle mechanical behaviour of reinforcement for main (longitudinal) reinforcement and stirrups, and includes statistics for time-dependent reduction in structural capacity and loss of cross-sectional area, conditional on beam collapse. This model is then used in a 1D random field analysis to calculate the extent of corrosion damage by Stewart and Suo (2009).

Spatial variability research carried out to date has been mainly focused on predicting the lifetime condition of a corroding structure and spatial variability of material, dimensional and environmental properties (Li et al. 2004; Karimi et al. 2005; Stewart 2005; Vu and Stewart 2005; Darmawan and Stewart 2007; Marsh and Frangopol 2008; Kenshel and O'Connor 2009; Akiyama et al. 2010; Zhai and Stewart 2010). A major shortcoming in the work carried out to date in this regard is that only

structural capacity and damage have been considered – the spatial variability and corresponding correlation associated with applied loads has not been allowed for.

The load models used to assess the safety of corroding structures are often either oversimplified or estimated from conservative standards or codes of practice and not from actual traffic data (Stewart 2004; Stewart and Al-Harthy 2008; Kenshel 2009). Analysis of measured data shows subtle patterns of correlation in vehicle weights and gaps, both within lanes and between adjacent lanes in same-direction traffic (OBrien and Enright 2011), which has not been accounted for in most of the literature. However, the greatest contribution to spatial correlation is the fact that the same heavy vehicle will cross all points on the bridge in its path of travel. Correlation between weights of vehicles are much weaker but do occur for a number of reasons. There are times during the day when heavy vehicles are more likely to travel (OBrien and Enright 2011). Further, vehicles from the same company sometimes choose to travel together and their weights can be highly correlated as they have similar payloads and operate under the same company policies.

A number of simplifying assumptions are made in the work by Nowak (1993). For instance, one in 15 heavy trucks has another truck side-by-side, and for one in 30 of these multiple truck events, the two trucks have perfectly correlated weights. Nowak (1993) defines a heavy truck as one with a Gross Vehicle Weight (GVW) in the top 20% of measured truck weights. It is found that two side-by-side trucks result in the maximum load effect in 75 years, with each truck having a GVW of 85% of the maximum individual GVW in 75 years. It has been noted that the assumptions on weight correlation are entirely based on judgment, as almost no data are available (Kulicki et al. 2007). OBrien and Enright (2011) show that correlated traffic gives a better fit to the measured data than models which assume no correlation. Their results lead to the conclusion that correlation may account for up to an 8% increase in lifetime maximum loading. It is also found that relative positions (gaps), within lane and inter-lane, have a significant influence on load effects for bridges with multiple same-direction lanes. For example, a truck in a fast lane is very often accompanied by a heavier truck in the adjacent slower lane.

The current study describes a time-dependent probabilistic-based resistance model which predicts probability of failure for chloride-induced corroding RC structures and correlation associated with traffic load. The objective of this study is to account for the effects of uncertainty and spatial correlation associated with the loading in combination with spatial correlation of resistance on the probability of failure over the bridge lifetime.

For this purpose two numerical examples are presented that illustrate these concepts. The first example starts with a simplistic load model. The simplistic model is a HL93 design load configuration, a moving three-axle truck and a uniformly distributed load (UDL), which has been modified using WIM data collected at the Netherlands. This model is used to emphasise the differences made by realistic traffic introduced in the second example. The realistic traffic load model is based on a traffic ‘scenario’ model (OBrien and Enright 2011). Scenarios consisting of several vehicles and all the associated properties, including weights and relative positions, are extracted from WIM data and perturbed using Kernel Density estimation. The simulation is run for many years and the correlations between traffic parameters (e.g., GVW, inter-vehicle gap) are implicitly included in each scenario. The resistance model of a two-lane simply supported RC slab bridge is the same in both examples to highlight the influence of the realistic load model on probability of failure. The effect of pitting corrosion and consequent loss of reinforcement cross-sectional area is taken into account through a 2D spatially variable time-dependent resistance model. It has to be noted that the distribution of load effect through the depth is not considered in this study.

In order to study the effect of correlation on load effect distributions and eventually probability of failure, three patterns of correlation with a range of correlation coefficients are studied in the first example and the results are compared to the actual correlation associated with the realistic traffic load model.

In the two examples considered in the current study, the random variables include loads in each lane, reinforcement cross-sectional area, concrete top cover and concrete strength, at each segment of the bridge longitudinally and in each lane. Other factors such as cracking, delamination, pot-holes, shrinkage and freeze/thaw are not considered and are beyond the scope of this study.

3 Random Field Modelling

Random Field Discretisation

As discussed, in a spatially variable analysis, the structure (or structural component) is discretised into a number of segments and a random variable is used to represent the random field over each segment. There are numerous methods for the discretisation of a random field. These may be classified based on their approach as one of three methods: (i) the midpoint method, (ii) the spatial averaging method and (iii) the series expansion method (Der Kiureghian and Ke 1988; Matthies et al. 1997). In the midpoint method the value of the random field over a segment is represented by its value at the centre (midpoint). It is a simple and robust approach to discretisation, for both Gaussian and non-Gaussian random fields. While it has been suggested that it tends to over-represent the variability of the random field (Sudret and Der Kiureghian 2000), it is chosen here due to its popularity among researchers.

The size of each segment has to be small enough to ensure that random properties are constant within it. The size of the discretised segment is usually defined based on practical and analytical considerations (Sterritt et al. 2001). The use of a fine mesh can significantly increase the computational effort for little improvement in accuracy. Further, the smaller segment size can result in numerical difficulties in the orthogonalisation of the covariance matrix. Conversely, if the segment size is too large the correlation between segments becomes negligible.

Autocorrelation Function

The spatial correlation between discretised segments in a random field analysis can be described by the correlation function (sometimes called the autocorrelation function) which defines the pattern of decay of the variance (Haldar and Mahadevan 2000). The correlation function $\rho(\tau)$ defines the correlation coefficient between two segments separated by distance τ in a random field. Various types of correlation function have been proposed (Vanmarcke 1985; Haldar and Mahadevan 2000) including triangular, exponential and Gaussian (or squared exponential) functions. The Gaussian function is the most widely used model in the literature (Li and Der Kiureghian 1993; Kersner et al. 1998; Haldar and Mahadevan 2000; Vu 2003; Li et al. 2004; Malioka and Faber 2004; Stewart 2006; Sudret et al. 2007) and is adopted here. It can be described (Vanmarcke 1985) as:

$$\rho(\tau) = exp\left(-\left(\frac{\tau_x}{d_x}\right)^2 - \left(\frac{\tau_y}{d_y}\right)^2\right) \quad (1)$$

where $d_x = \theta_x/\sqrt{\pi}$; $d_y = \theta_y/\sqrt{\pi}$ and θ_x, θ_y are scales of fluctuation (i.e., the distances over which correlation persists in a random field) in x and y directions respectively.

The parameters, $\tau_x = x_{j+1} - x_j$, $\tau_y = y_{j+1} - y_j$ are distances between centres of segments j and $j+1$ in the x and y directions respectively (Vanmarcke 1985).The terms d_x and d_y have been described elsewhere as the correlation lengths (Kersner et al. 1998; Vu 2003) or the correlation radii (Malioka and Faber 2004). In this study, a constant, ρ_0 is also applied to the correlation function to account for a baseline level of correlation amongst all segments of the random field, independent of distance. Thus, the correlation between segments is described by:

$$\rho(\tau) = \rho_0 + (1-\rho_0)exp\left(-\left(\frac{\tau_x}{d_x}\right)^2 - \left(\frac{\tau_y}{d_y}\right)^2\right) \quad (2)$$

The validation and calibration of correlation functions requires large amounts of spatial data that is difficult to obtain and, as such, engineering judgment is often used to match a correlation function to a particular random field.

The value of the measure of fluctuation, however, should be chosen in conjunction with an appropriate random field segment size so that mathematical and computational difficulties are avoided. It is suggested that the size of the segments should be one fourth to one half of the correlation length (Der Kiureghian and Ke 1988). Therefore for a correlation length of 3.0 m (i.e., scale of fluctuation = $3\sqrt{\pi}$), a segment size of 1.5 m or less is recommended.

4 Time-Dependent Spatially Variable Resistance

The cross sectional area of the reinforcement in an RC member is reduced as corrosion progresses, which leads to a reduction in the load carrying capacity of individual segments. Recent studies on safety and structural reliability of corroding reinforced concrete beams, assume general (uniform) corrosion and generally, simplified assumptions are made for pitting corrosion which ignore the spatial variability associated with pitting along the reinforcing bar (Mori and Ellingwood 1993; Rodriguez et al. 1997; Stewart and Rosowsky 1998; Mangat and Elgarf 1999; Vu and Stewart 2000; Torres-Acosta and Martinez-Madrid 2003; Coronelli and Gambarova 2004). Stewart (2004) proposes a stochastic model to take account of the spatial effect of pitting corrosion on structural reliability. This model is used here to account for the loss of cross-sectional area of a reinforcing bar.

The loss of reinforcement diameter under uniform corrosion can be described using Faraday's Law. The law indicates that if the corrosion rate is assumed to be constant over time, then the remaining cross-sectional area of corroding main reinforcement after *t*-years, $A_{s,uni}(t)$, can be estimated as:

$$A_{s,uni}(t) = \sum_1^{n_b} \frac{\pi[D_0 - \Delta D_i(t)]^2}{4} \quad (3)$$

where, n_b is the total number of reinforcing bars, D_o is the original bar diameter and $\Delta D(t)$ is the reduction in bar diameter given by:

$$\Delta D(t) = 0.0232 i_{corr}(t - T_i) \quad (4)$$

where, i_{corr} is corrosion rate and T_i is the time in years to corrosion initiation (i.e., the time for chloride ions to penetrate through the concrete cover from the surface and reach a critical (threshold) value at the level of the reinforcement).

The extent of pitting corrosion is defined by the pitting factor, *R*, which is given as:

$$R = p(t)/p_{av}(t) \tag{5}$$

where $p(t)$ is the maximum pit depth and p_{av} is the penetration calculated based on general corrosion, which is time-dependent and can be written as:

$$p_{av}(t) = \Delta D(t)/2 \tag{6}$$

Stewart (2004) applies extreme value theory to predict maximum pit depth as a function of reinforcement bar and length. Improved extreme value statistics for pitting is achieved by including the effect of corrosion on reinforcement material properties (Stewart and Al-Harthy 2008). Maximum pit depths, $p(t)$, are measured for each 100 mm length of the reinforcing bar. A Gumbel distribution is selected to fit to the R values extracted from the measurements (Stewart and Al-Harthy 2008). The statistical parameters are modified to predict the distribution for any length of reinforcement bar, L_u:

$$\mu_R = \mu_{R_0} + \frac{1}{\sigma_{R_0}} \times \log\left(\frac{L_u}{L_0}\right) \tag{7}$$

$$\sigma_R = \sigma_{R_0} \tag{8}$$

where, μ_{R_0} and σ_{R_0} are Gumbel parameters obtained from corrosion tests for reinforcing bars of length $L_0 = 100$ mm (Sheikh et al. 1990; Stewart 2009). It is assumed the adjacent reinforcing bars are statistically independent which is not the case in reality, but the statistical parameters taken from measurements have captured this variability (Stewart and Al-Harthy 2008).

In order to take account of the loss of cross-sectional area for the reinforcing bar due to pitting corrosion, an assumption regarding the pit shape has to be employed. The pit shape shown in Figure 1 (Val and Melchers 1997) is applied in the current work.

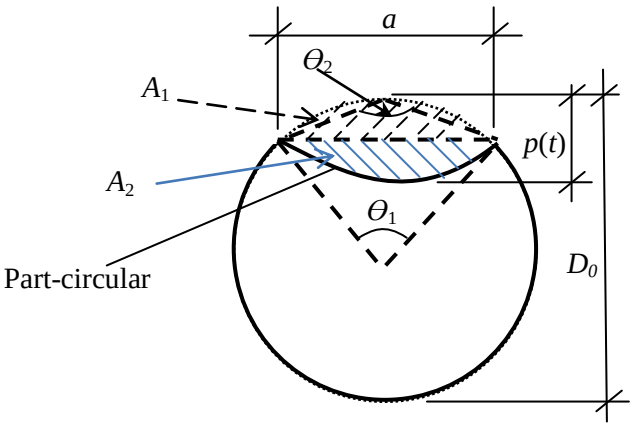

Figure 1- Pitting corrosion

The reduced cross-sectional area of a single corroding bar at any time t, under pitting corrosion (Figure 1), can be calculated as follows (Val and Melchers 1997):

$$A_{pit}(t) = \begin{cases} A_1 + A_2 & p(t) \le D_0/\sqrt{2} \\ \pi {D_0}^2/4 - A_1 + A_2 & D_0/\sqrt{2} < p(t) \le D_0 \\ \pi {D_0}^2/4 & p(t) > D_0 \end{cases} \tag{9}$$

with:

$$A_1 = \frac{1}{2}\left[\theta_1 \left(\frac{D_0}{2}\right)^2 - a\left|\frac{D_0}{2} - \frac{p(t)^2}{D_0}\right|\right] \quad (10)$$

$$A_2 = \frac{1}{2}\left[\theta_2 p(t)^2 - a\frac{p(t)^2}{D_0}\right] \quad (11)$$

$$a = 2p(t)\sqrt{1-(p(t)/D_0)^2} \quad (12)$$

$$\theta_1 = 2\sin^{-1}(a/D_0) \quad (13)$$

$$\theta_2 = 2\sin^{-1}[a/(2p(t))] \quad (14)$$

Resistance models can be derived from first principles or adapted with reference to design/assessment codes applicable to the structure under consideration (Kenshel and O'Connor 2009). In the current study, moment capacity is calculated according to the American bridge design specification (AASHTO 2012) and taking account of model error. Assuming a rectangular non-prestressed member, the time-variant nominal flexural resistance of an RC beam is:

$$M_n(t) = ME{\times}A_s(t)f_y(t)d\left(1 - \frac{f_y(t)A_s(t)}{2\eta f_c bd}\right) \quad (15)$$

$$A_s(t) = \sum_{i=1}^{n_b}\left(\frac{\pi {D_0}^2}{4} - A_{pit_i}(t)\right)$$

where, $A_s(t)$ is the time-dependent area of reinforcement, $f_y(t)$ is the steel yield strength, f_c is concrete compressive strength, b is width, d is effective depth, *ME* is model error which considers the statistical uncertainly associated with empirical modelling and η is a factor to define the effective depth of the compression zone. Statistical independence of pitting is assumed for each reinforcing bar.

The yield stress reduces linearly according to Du et al. (2005) and Stewart (2009):

$$f_y(t) = \left(1.0 - \alpha_y \frac{A_{stnom} - A_s(t)}{A_{stnom}}\right) f_{y0} \quad (16)$$

where f_{y0} is the yield stress of an uncorroded reinforcing bar, α_y is an empirical coefficient, and

$$A_{stnom} = n_b \times \pi \frac{D_0^2}{4}. \quad (17)$$

Reliability of an engineering system refers to the probability of survival or the complement of probability of failure (Melchers 1999). The concept of a limit state is used to define 'failure' in the context of structural reliability analysis. The term 'failure' in a reliability analysis does not necessarily imply structural collapse, but in most cases refers to a situation when the performance of the structure falls short of a predefined limit. For example, if the limit state to be considered is the initiation of reinforcement corrosion, then failure in this case may be defined as when the chloride content at the reinforcement exceeds a critical value. In this paper, failure is defined as when the load effect at any segment in the structure has exceeded the resistance or capacity.

The performance criterion is that the resistance must exceed the effect of load:

$$G = R - S \geq 0 \quad (18)$$

where R is resistance and S represents load effect. Theoretically, the solution of Equation 18 can be obtained through one of the following three methods (Melchers 1999): (i). direct analytical integration; (ii). numerical integration or, (iii). by transforming the integrand into a multi-normal joint probability density function for which results for some special cases are readily available.

Except for some special cases, the integration of Equation 18 over the failure domain, $G \leq 0$, cannot be performed analytically (Melchers 1999). One common example of a type 2 method is Monte Carlo (MC) simulation. As for type 3 methods, there are several classical techniques such as the FORM and SORM. These methods have been described in detail by many authors (Melchers 1999; Haldar and Mahadevan 2000; Ang and Tang 2007).

In this study, Monte Carlo simulation is used to generate load (which results in load effects at each element when combined with influence lines) and resistance, from the defined model, for each segment of the random field. In the next step, performance criteria are checked for each segment for all generated load and resistances. Then the violations of the performance criterion are used to define the probability of failure for the given load and resistance model. It is found that 2.5×10^5 simulations results in accurate estimation of probability of failure (less than 1% error) for the studied load and resistance model in the two examples.

5 Illustrative Examples

This section presents results from a spatial time-dependent reliability analysis of a simply supported RC slab bridge of 20 m length, 10 m width and 1 m depth. In the first example, a notional probabilistic load model is used to demonstrate the nature of the problem. In the second example, the same bridge is presented under realistic simulated traffic loading with associated load correlations based on measured scenario data.

Figure 2.a is a schematic illustration of the solid slab bridge deck discretised into 0.5 m × 0.5 m segments. Bold dashed lines in the figure correspond to the wheel tracks. All wheel loads are assumed to be 2 m apart, transversely, with the truck situated in the centre of the lane. A finite element model of the solid bridge deck was built in the MD Patran software (Figure 2.b). In the finite element analyses, the slab is modelled using plate elements with both bending and membrane capabilities, i.e., six degrees of freedom per node. This model is used to generate influence lines of bending moment for each of the 800 elements due to a single axle load moving on each lane (i.e., each element has two influence lines and there are 800×2 influence lines in total). These influence lines are then used to generate bending moment due to random loading on the bridge.

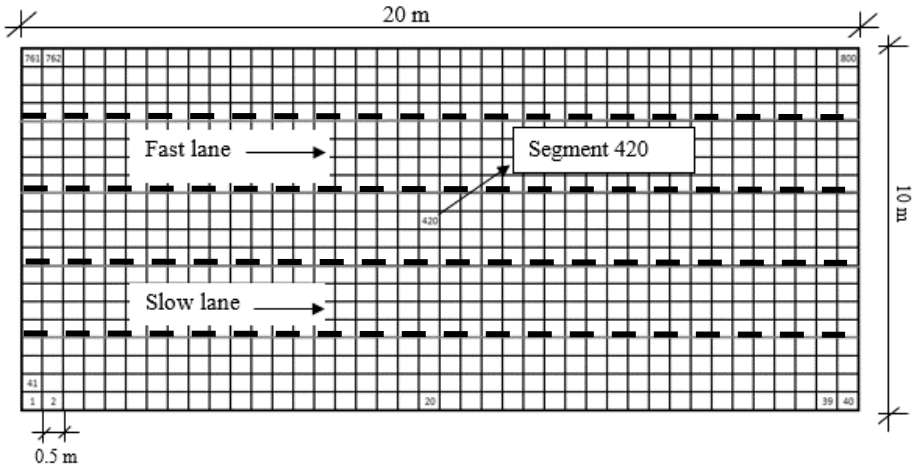

a. Plan view of discretised slab bridge deck

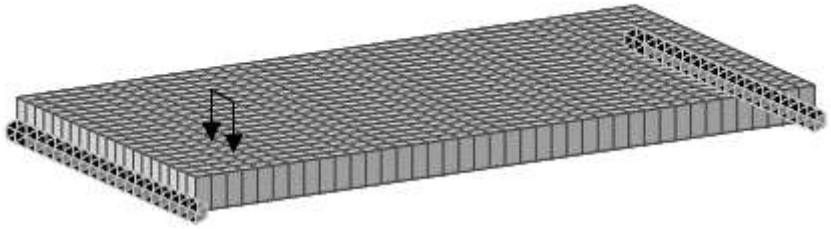

b. Finite element model

Figure 2 - Slab bridge deck of 20m length and 10m width

6 Slab Bridge under Notional Probabilistic Traffic Model

Analysis of the measured data collected by WIM sensors installed in 5 European countries, shows subtle patterns of correlation in vehicle weights and gaps, both within lanes and between adjacent lanes in the same-direction traffic. It appears that a heavy truck in the fast lane tends to be associated with a nearby truck in the slow lane, i.e. it is passing another truck. For short to medium span bridges, loading events featuring one truck in each lane (either side-by-side or staggered) are particularly important. The first example will assess possible patterns of dependence between the weights of these vehicles, and the gap between the two vehicles. This example models the slab bridge under a notional probabilistic traffic model with a correlation coefficient associated with the GVWs and the gap between front axles. Three scenarios of correlation are assessed to illustrate the importance of each pattern in probability of failure.

This example also incorporates the effect of time-dependent spatially variable pitting corrosion. It shows the implications of considering spatial variability in a structural reliability analysis for deteriorating RC bridges in flexure, as well as the effect of correlation associated with vehicle weights between adjacent lanes.

Load Modelling

Like the HL93 design load, the probabilistic traffic load model consists of a uniformly distributed loading (UDL) and a 3-axle truck load. The truck (Figure 3) consists of six vertical concentrated loads at 4.5 m intervals longitudinally and 2 m transversely. WIM data collected in the Netherlands has been used as a basis for this notional load model. Statistical parameters are obtained here by trial and error and chosen to give the cumulative probabilities of bending moment that approximately match those found due to collected WIM data. The WIM database consists of 650 000 trucks, weighed over a 20 week period in 2005 at Woerden (Enright 2010). For this purpose, bending moment at mid-span of a simply supported beam (1D) is calculated for two lanes of measured traffic (i.e., bending moment at mid-span due to traffic on the slow lane and bending moment at mid-span due to traffic on the fast lane only). The resulting distribution is used as a benchmark to find the best parameters for the notional load model. The distribution used for the notional load model is assumed to be GEV which has been widely used in the literature for traffic load modelling. It has to be noted that the 1D mid-span bending moment is only used to find the notional load properties. For the load effects at each segment, the notional load model is applied to the influence lines resulting from the 2D finite element model. In order to drive the notional load model in each lane, the effect of traffic on the other lane is ignored. This assumption underestimates the load on each lane but it is found that the magnitude of load is a non-contributing factor in the influence of correlation on probability of failure.

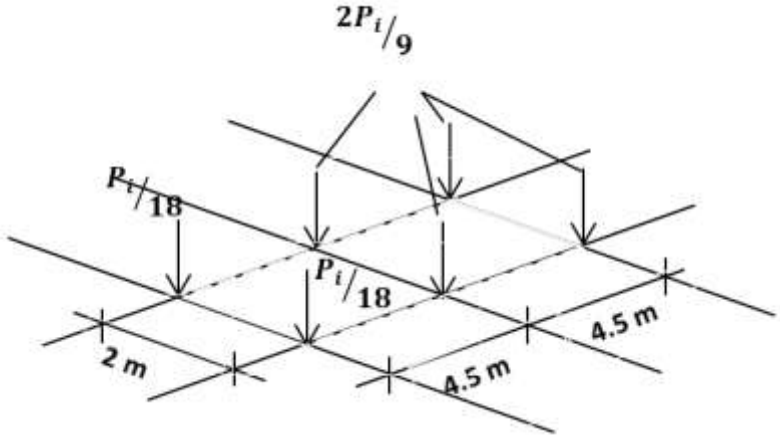

Figure 3 - Idealised truck live load model

Figure 4 illustrates the distributions that result from the notional traffic load model and WIM data on the 20 m bridge on a Gumbel scale plot (i.e., double log of cumulative distribution function). In this figure, S1-HL93 is the mid-span bending moment calculated in the slow lane due to the notional truck model, given the parameters in Table 1, and S1-WIM is the bending moment due to actual traffic using WIM data. S2-HL93 and S2-WIM are distributions due to notional HL93 and WIM data in the fast lane respectively. It can be seen from the figure that the parameters used for both lanes are giving a very good match (i.e., less than 1% mean squared error) to those found from WIM data. The optimised parameters are given in Table1.

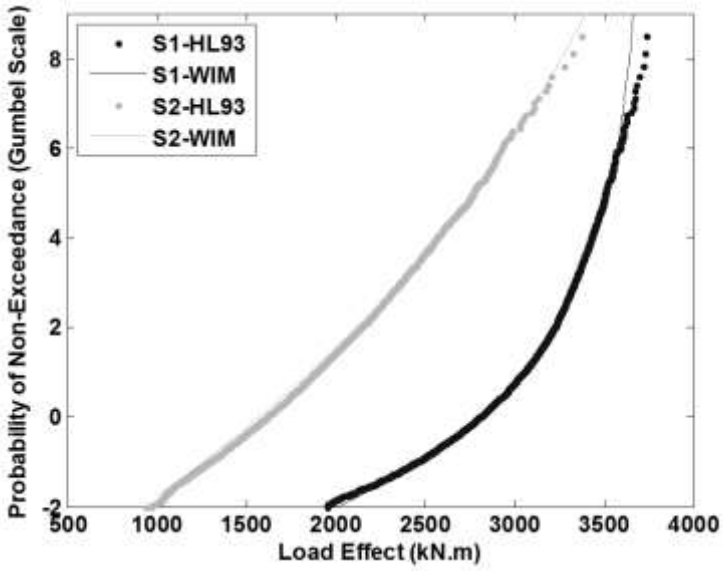

Figure 4 - Mid-span bending moments for notional load model and measured WIM data

Table 1 – Parameters of Generalised Extreme Value distribution for traffic load model

	μ	σ	ξ
Truck GVW in Slow-Lane (P_1 - Figure 5) (kN)	620	75	-0.4
Truck GVW in Faster Lane (P_2 - Figure 5) (kN)	300	75	-0.1
Uniformly Distributed Load (UDL) (kN/m)	9	1.5	0

Monte Carlo simulation is used to generate combinations of UDL's and GVW's for trucks. The gap between the two loads, d (i.e., from rear axle of leading truck to front axle of following truck), is taken from a uniform distribution with range (-10 m, +10 m). Each load scenario includes P_1, P_2, d (Figure 5) and UDL. For each loading scenario generated, the load effect (bending moment in this study) is calculated using the influence lines found from the finite element model (i.e., each (P_1, P_2, d) combination is passed over the bridge in steps of 0.5 m, to obtain the maximum load effect at each segment). It is assumed that the load characteristics do not change during the bridge lifetime (i.e., no time-dependent change in vehicle weights or traffic volume).

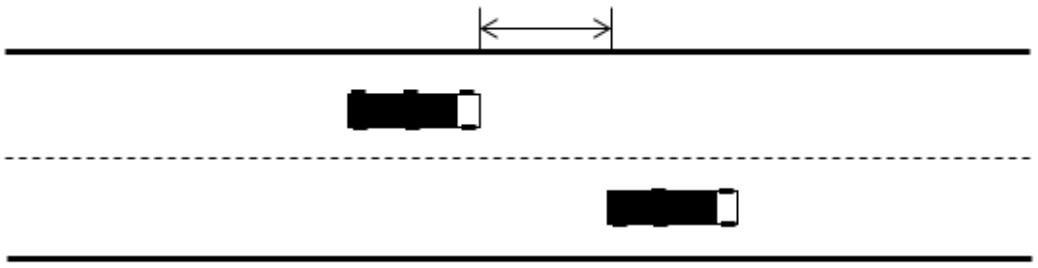

Figure 5 - Statistical parameters used for notional load model

In this example, three types of correlation are introduced to examine the effect of correlation: type 1. correlation between GVW of the two trucks; type 2. correlation between the gap and GVW of truck in the slow lane and type 3. correlation between the gap and the GVW of the truck in the fast lane. These scenarios cover all possible correlation patterns for two trucks in two lanes of same-directional traffic.

In order to assess the sensitivity of load effect distribution to correlation coefficient of GVWs and gaps, a range of correlation coefficients is considered. For each scenario, the correlation coefficient is varied from -50% to 50% to illustrate the influence of correlation on load effect resulting from each scenario. Figure 6.a to Figure 6.c illustrate bending moments (due to traffic load only) at segment no. 420 (mid-span) due to the three correlation patterns and varying correlation coefficients. In these figures the solid black corresponds to ρ = -50% and as the colour changes towards the grey spectrum, the ρ increases (i.e., lightest grey corresponds to ρ = +50%).

It can be seen from the figures that the first pattern of correlation (i.e., correlation between GVWs) causes the highest variation in bending moment distribution. Figure 6.d shows the variation in 75-year characteristic value for each pattern, varying the magnitude of the correlation coefficient. It can be seen that the first pattern resulted in a 1% increase in characteristic value for 10% increase in correlation coefficient between GVWs of the two trucks. The other two patterns do not show any particular trend due to variation in ρ. Given the increase in characteristic load effect, the first correlation pattern is used for further analysis in this study.

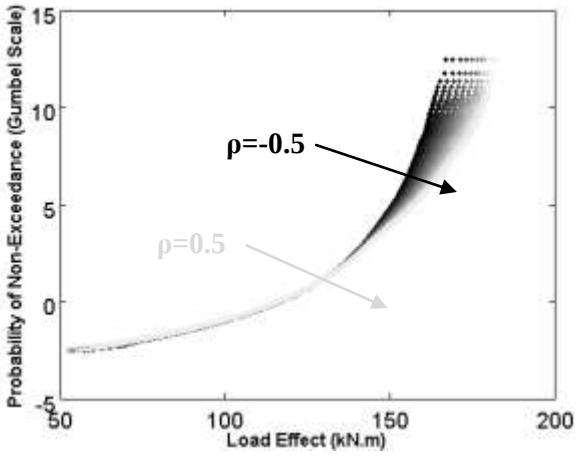

a. **Bending moment at segment 420 due to live load only - correlation type 1**

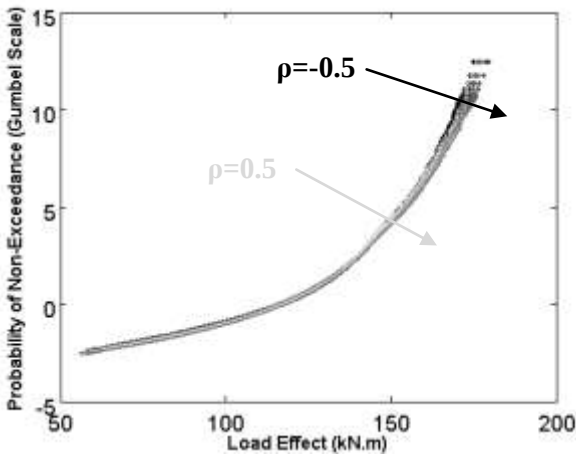

b. **Bending moment at segment 420 due to live load only - correlation type 2**

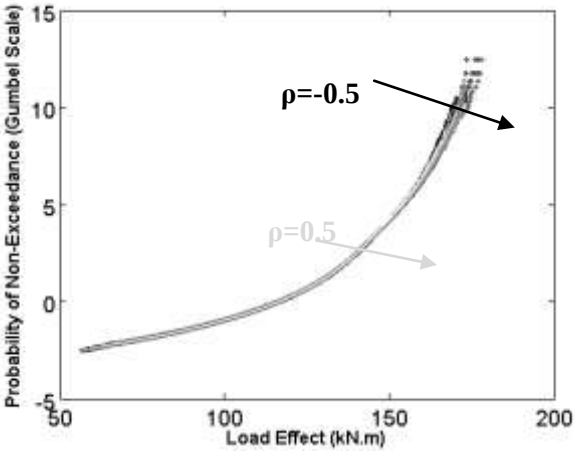

c. **Bending moment at segment 420 due to live load only - correlation type 3**

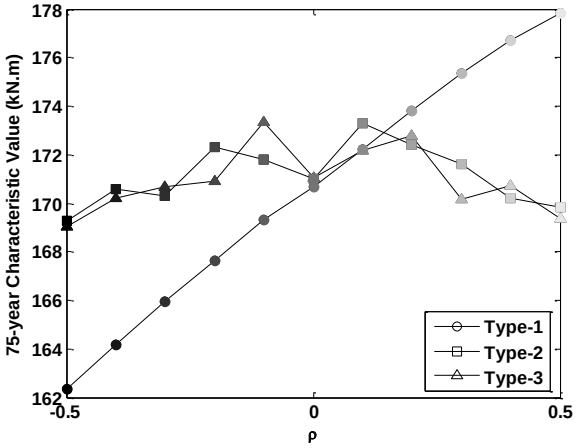

d. **75-year characteristic value**

Figure 6 - Load effect at segment 420 due to live load only

Figure 7.a. illustrates the load effect distribution given the first pattern of correlation for element no. 420, taking account of self-weight of concrete with density, 2400 kg/m^3 (i.e., dead load + traffic load). It can be seen that by adding self-weight to the traffic load bending moment, the variation due to correlation coefficient of GVWs reduces in the cumulative distribution. Figure 7.b shows that a 10% increase in GVW correlation results in a 0.1% increase in the 75-year characteristic value (i.e., 10 times less than the variation in load effect due to traffic load only). This can be explained by the fact that the bending moment due to self-weight is the main part of the load effect at each segment. The self-weight is constant for all segments so it does not contribute to an increase in characteristic value due to correlation.

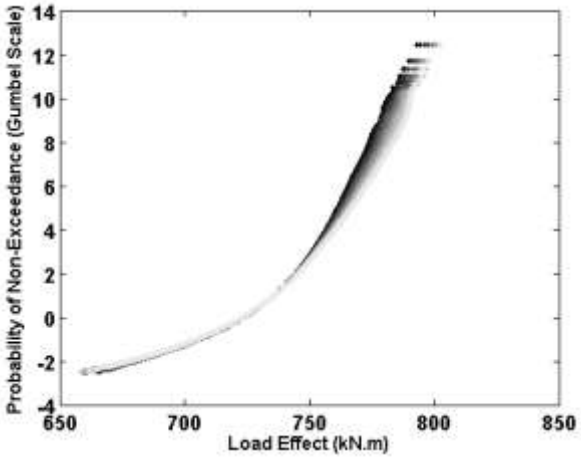

a. Cumulative distribution due to dead and live load

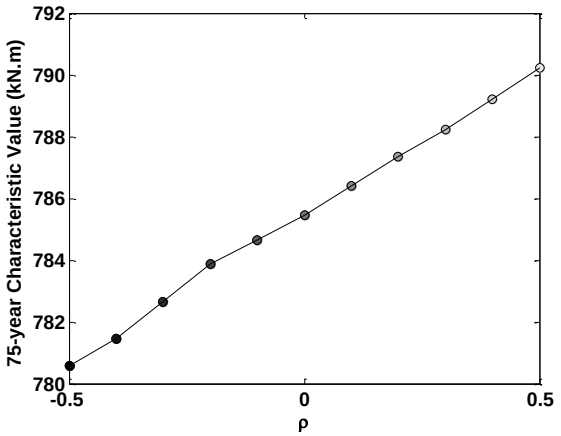

b. 75-year characteristic value due to dead and live load

Figure 7 - Bending moment at segment 420 due dead and live load

It is found that load effect distributions are highly correlated (i.e., correlation coefficient greater than 88%). It has to be noted that this correlation is a result of correlation between influence lines rather than the correlation coefficient of GVWs. Figure 8 shows the correlation coefficient patterns of load effects for segment nos. 402 to 420 to illustrate the correlation variation pattern for three correlation coefficients of GVW's: -50%, 0 and 50%. It can be seen that the minimum value of correlation coefficient of load effect is 0.88 between element 440 and other elements which could be a result of local effects. The general pattern seems to be consistent although it can be seen that the lighter area (i.e., area with higher correlation) expands slightly as the correlation coefficient of GVW's increases. This figure suggests that the load effect correlation is governed by correlation between the influence lines (i.e., load sharing).

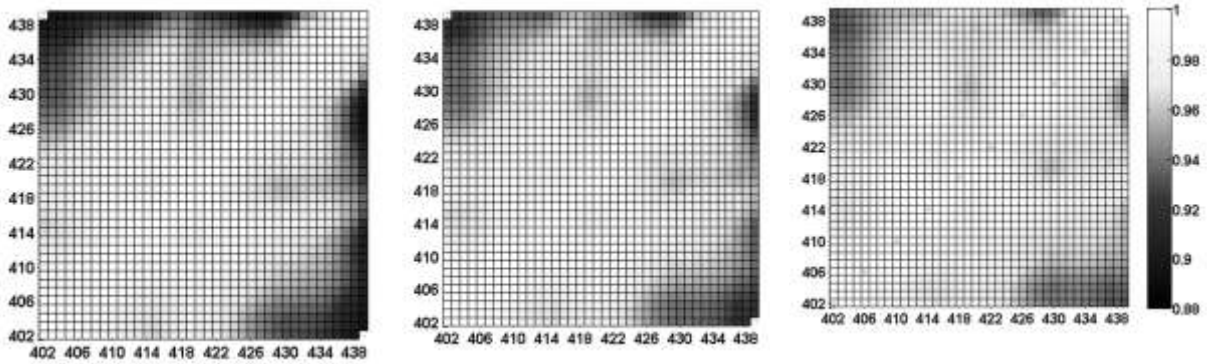

a. ρ = -50% b. ρ = 0% c. ρ = 50%

Figure 8 - Correlation coefficient pattern for elements 402 to 420 (see Figure 2 for element nos.)

Resistance Modelling

The resistance of each segment is a function of many variables. These are varied randomly with the distribution properties given in Table 2. The random field variables are correlated using the autocorrelation function given in Equation 2 with assumed $d_x = d_y = 1$ m for cover and concrete compressive strength. The constant correlation term, ρ_0, in Equation 2 is varied from 0 to 50% to compare the effect of correlation coefficient for resistance to correlation coefficient for load using approximately the same amount of correlation. For each realisation, data is generated for each segment using the parameters given in Table 2. By applying Equations 3 through 17, the resistance at each segment is calculated over time. The time before corrosion initiation is not considered in this study, i.e., time is measured from the instant of corrosion initiation. Monte Carlo simulation is used to find the resistance distribution for each segment in each year.

Table 2 – Probability distribution properties for resistance parameters.

Random Field Variables	Definition	Mean, μ	Standard Deviation, σ	Distribution	Variability	References
f_{ck} (MPa)	Concrete cylinder strength	47.5	6	Normal	Random Field	Attard and Stewart (1998)
k_w ($f_c = k_w \times f_{ck}$)	Workmanship factor	0.87	0.052	Normal	Random Field	Stewart (1995)
C (mm)	Concrete Cover	51.6	5.78	Normal	Random Field	Van Daveer (1975); Attard and Stewart (1998)
i_{corr} (μA/cm^2)	Corrosion rate	1	---	---	Constant	-------
f_{y0} (MPa)	Yield strength of an un-corroded reinforcing bar	500	---	---	Constant	-------
L_u (mm)	Reinforcing bar length	500	---	---	Constant	-------
L_0 (mm)	Reinforcing bar length from experimental data	100	---	---	Constant	Stewart and Al-Harthy (2008)
D_0 (mm)	Reinforcing bar initial diameter	24	---	---	Constant	-------
h (m)	Depth	1.0	---	---	Constant	-------
ME	Model Error	1.02	0.06	Normal	Random	Vu (2003)
n_b	Number of bars per segment	5	---	---	Constant	-------

Statistical parameters used for the pitting factors for 24 mm bars are shown in Table 3.

Table 3 - Statistics of pitting corrosion

Reinforcing bar diameter	Gumbel parameters		
D_0 (mm)	μ_0	σ_0	Reference
24	6.55	1.07	Stewart and Al-Harthy (2008)

Figure 9 illustrates the time-dependent nature of the resistance distribution for the 420th segment for zero correlation coefficient. In this figure, the black curve corresponds to the resistance distribution in the 1st year after corrosion and as the time goes by, the distribution is shown in shades of grey (the solid black distribution corresponds to year 50). It can be seen that, as time since corrosion initiation progresses, the mean resistance falls, as expected (from black peak to lightest grey peak). Also, the standard deviation increases with time, i.e., the resistance becomes more variable. It has to be noted that in this study the variation in resistance within each year is ignored (i.e., resistance distribution is assumed constant throughout the year for each individual year).

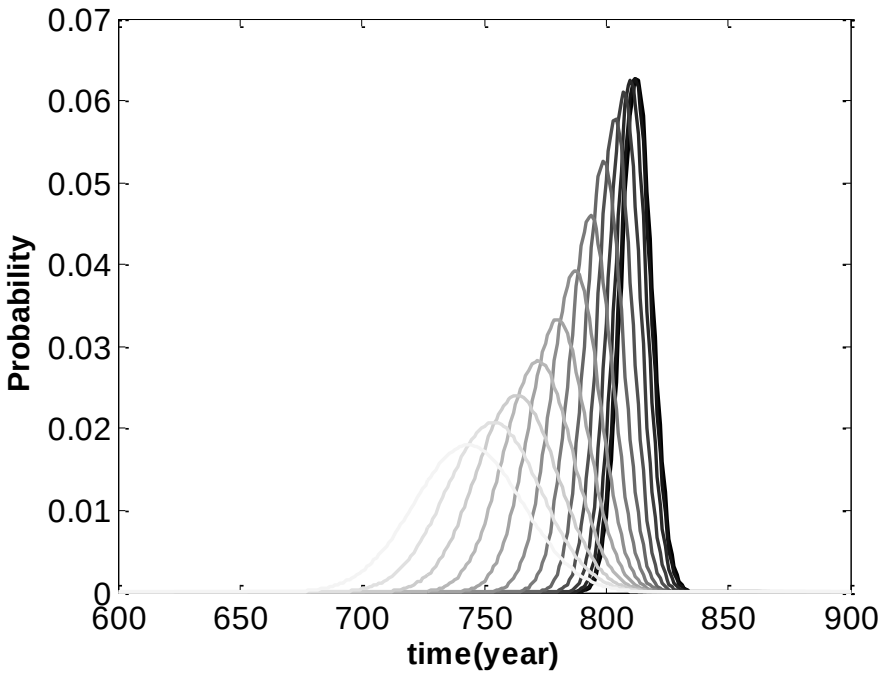

Figure 9 - Time-dependent resistance distribution for 420th segment

Figure 10 illustrates the variation of the cumulative distribution of resistance at segment no. 420 for correlation coefficient varying from 0 to 50% (black corresponds to 0 and lightest grey represents 50% correlation). It can be seen that the increase in correlation coefficient does not result in any significant trend in the resistance distribution.

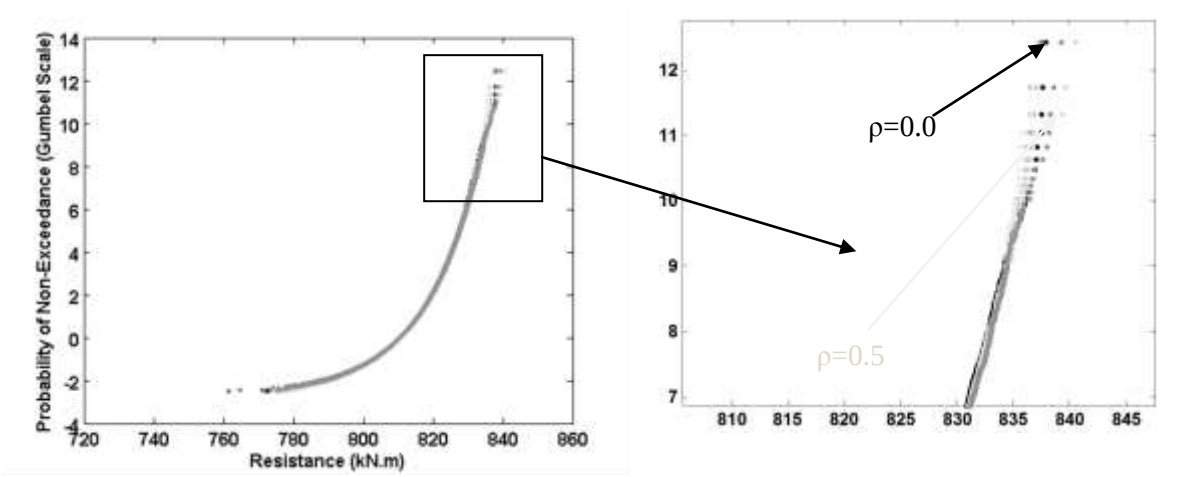

Figure 10- resistance distribution for 420th segment-1st year after corrosion

It is found that the correlation coefficient has a strong influence on the correlation of resistance between adjacent elements (i.e., correlation coefficient of resistance in adjacent elements is increased by 10% due to an increase of 10% in correlation coefficient of resistance parameters). Figure 11 illustrates correlation coefficient between resistance distributions generated for elements 401 to 420. Figure 11.a corresponds to a correlation coefficient of 0 and Figure 11.b shows correlation coefficients of resistance for 50% increase in correlation in resistance parameters. It can be seen from this figure that the lighter area is significantly extended towards adjacent elements (i.e., correlation coefficient of resistance distribution in adjacent elements is increased, as expected).

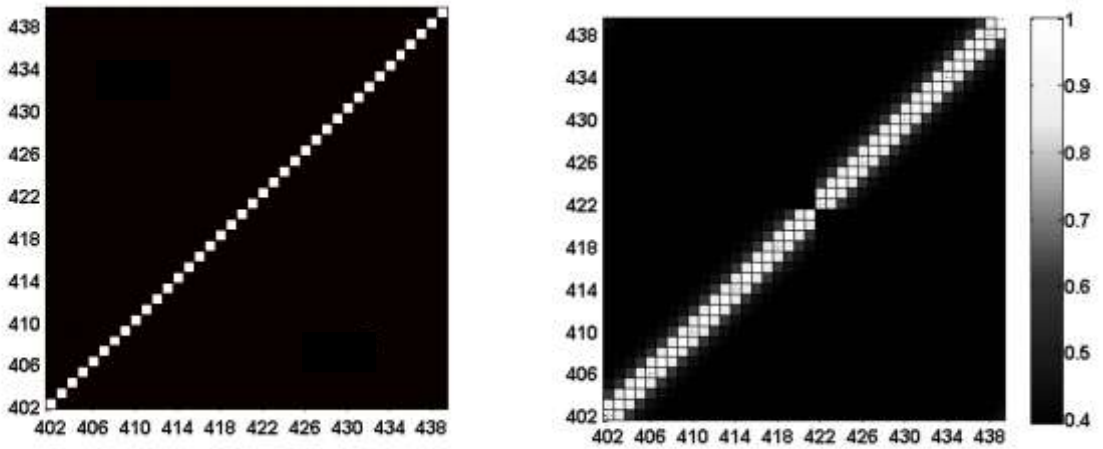

a. ρ = 0% b. ρ = 50%

Figure 11 - Correlation coefficient of resistance between elements 401 to 440

Probability of Failure

In order to study spatial variability in a reliability analysis context, correlation coefficient of 10% is used for both load and resistance. For this purpose the parameters introduced in Tables 1 and 2 are used to generate notional load and resistance models and the combination of correlated and uncorrelated load and resistance models is examined (i.e., each element has two sets of load and resistance: correlated and uncorrelated). Based on applied bending moment and resistance calculated at each segment for each set of parameters, the difference, $R - S$ is determined and the segments are considered to have failed if $R - S$ results in a negative value (given the 2.5×10^5 number of simulations, each segment has 2.5×10^5 load effects and $2.5\times10^5\times50$ (year) resistance values).

It is found that the definition of failure is another contributing factor that has to be considered. For this study, it is assumed that the bridge fails if at least *m* elements fail (i.e., resistance of the elements being less than load effect) in the structure. The *m* value is varied from 1 element to 40 elements to study the effect of the definition of failure.

Figure 12 illustrates the progression of probability of failure per day throughout the life of the structure, for correlated load and resistance based on different definitions of failure. The darkest curves in Figure 12.a correspond to the probability of failure given that at least 1 element has failed in the bridge. The curves are shown by lighter shades of grey as the number of elements required for failure increases (i.e., the lightest corresponds to the probability of failure given that at least 40 elements must fail). This figure shows that the probability of failure converges as the number of elements required for failure increases, as expected.

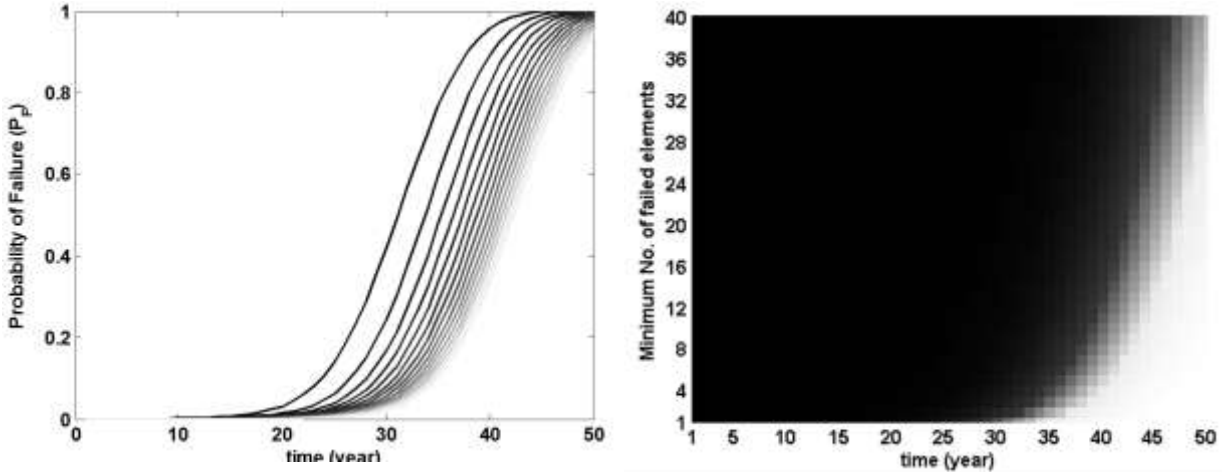

a. Probability of failure for different definitions

b. Contour plot

Figure 12 – Probability of failure for correlated load and resistance

Figure 13 shows the probability of failure for all combinations of correlated and uncorrelated load and resistance: 1. correlated load and correlated resistance (CL-CR), 2. correlated load and uncorrelated resistance (CL-IR), 3. uncorrelated load and correlated resistance (IL-CR) and 4. uncorrelated load and uncorrelated resistance (IL-IR). Figure 13.a illustrates the probability of failure for all combinations and 15 definitions of probability of failure (i.e., from at least one segment failing to at least 15 segments failing). It can be seen that the first group of results (i.e., failure being when at least one segment fails) shows no particular trend in the 4 combinations, as expected (i.e., single element failure cannot reflect the correlation of resistance and load effect in adjacent elements). In the second group, it is shown that the first combination (CL-CR) and fourth combination (IL-IR) give the highest and lowest probabilities of failure respectively. The difference between the highest and lowest probability is greater than 15%. This difference in the second group could be mainly the result of correlated load. However comparison in the 3rd to 15th groups shows that the IL-CR case generally gives higher probability of failure that CL-IR. A similar trend, though of smaller extent, can be seen for probability of failure in the 15th and 25th years after corrosion initiation in Figures 13.b and 13.c respectively. Figure 13 suggests that the influence of correlation on probability of failure is a function of time, definition of failure and load and resistance correlation levels. In the early stages where probability of failure is low, load and resistance correlation have the highest effect on the probability and as time progresses, this effect diminishes.

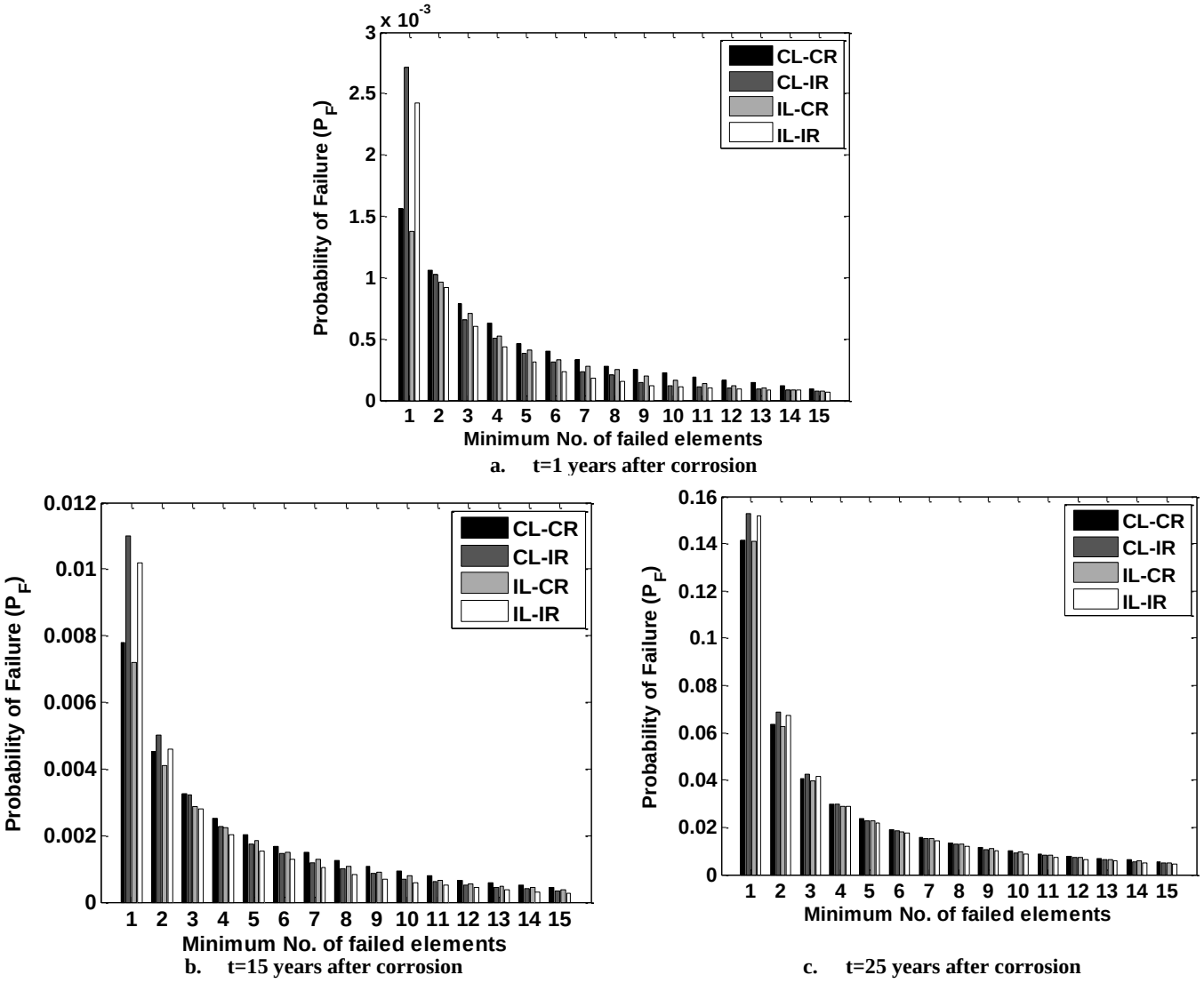

Figure 13 – Probability of failure for correlated and uncorrelated load and resistance

6.1 Slab Bridge under Realistic Traffic Load

In the second example in this study, the same single-span solid slab bridge is analysed under realistic traffic loading which is based on WIM records collected in the Czech Republic in 2007 and 2008. Monte Carlo simulation is used to generate streams of traffic, and scenario modelling is used to reproduce the correlations found in the measured traffic. A detailed description of the methodology for this scenario modelling approach is given by Enright (2010), and is summarized here. This model has been calibrated against extensive WIM data from different European countries.

Load modelling

A detailed analysis of the WIM measurements (Enright 2010) reveals that there are patterns of correlation and interdependence between vehicle weights, speeds and inter-vehicle gaps that may be significant for bridge loading. For example, it is found that there is a significant peak in average GVW in the fast lane when the inter-lane gap is around zero (OBrien and Enright 2011). By definition, gaps become smaller as traffic flow rates increase, but WIM measurements also exhibit some dependence between gaps and GVW (Enright and OBrien 2012). Speeds of vehicles in the same lane become highly correlated as inter-vehicle gaps reduce (Enright 2010).

Measured traffic and Monte Carlo simulation of traffic, with each lane being simulated independently, are used for characteristic load effect estimation in the Eurocode bridge load model (Bruls et al. 1996; O'Connor et al. 2001; Dawe 2003; EC1 2003). Although extrapolating from load effects calculated from measured traffic implicitly incorporates the patterns of correlation in the traffic, it suffers from high uncertainty due to the extrapolation process. Gindy and Nassif (2006) report up to 33% variation in results from extrapolation, and Dawe (2003) notes up to 20% variation in the characteristic load estimated for Eurocode.

OBrien & Enright (2011) propose a method for modelling multi-lane same-direction traffic and show that the significant weight and gap correlations identified in extensive WIM data are modelled correctly. The method works by dividing the WIM record for the site into 'scenarios', each containing between 5 and 8 slow-lane trucks, together with any adjacent trucks in the fast lane. To simulate traffic at the site, scenarios are repeatedly selected at random from the WIM data. For each scenario, the truck weights and inter-truck gaps are varied using kernel density estimators (Silverman 1986). With this smoothed bootstrap method (De Angelis & Young 1992) each parameter of the selected scenario is slightly perturbed to create a new scenario with similar properties to the original, while maintaining gap and weight correlations. The bandwidth used in kernel density estimation controls the amount of variation which is applied to the original scenario. The bandwidth selection used by OBrien & Enright (2011) is acknowledged to be somewhat arbitrary and there is a risk that a small quantity of unrealistic driver behaviour is being created. For example, a situation may be created where a fast lane truck is moved to a position where it would normally have returned to the slow lane. In this study, Scenario Modelling is concerned only with the trucks in the WIM data; the cars are ignored as they are considered insignificant for short-span bridge loading.

In the simulation, randomly selected scenarios are placed in the traffic in sequence, with the last truck in one scenario being replaced by the first truck in the following scenario. This preserves the appropriate gap distributions, but care needs to be taken to avoid a very light truck replacing a heavy truck or vice versa. This is achieved when extracting scenarios from the WIM data by specifying that the first and last slow-lane truck in the scenario must have a gross vehicle weight (GVW) less than 30 tonnes. These lighter trucks are assumed not to be significant for critical bridge loading and therefore swapping one of these trucks for another will not affect the characteristic load effects obtained from simulation.

A sample scenario is shown in Figure 14. In each scan, if the last truck is greater than 30 tonnes then more trucks are included until the scenario can finish on a slow-lane truck which is less than 30 tonnes (OBrien & Enright 2011). The different scans allow for more variation in the scenarios and capture more scenario configurations.

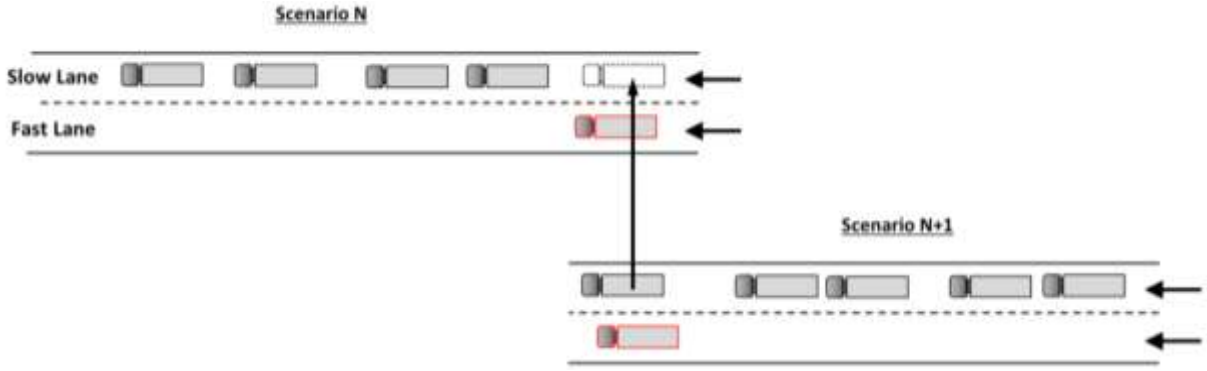

Figure 14 - Example for sampled traffic scenario

In the simulation, a scenario is selected randomly from all scenarios corresponding to the flow rate for the time of day. In this way, the measured relative frequencies of the parameters of scenarios (i.e., GVW, gaps, speed and flow rate) are reproduced in the simulation. The process is extended to generate scenarios that have not been directly observed. Gap combinations different from those observed and vehicles heavier than any measured are of particular interest. This is taken into account by applying random 'noise' to the data using variable-bandwidth kernel functions. Scott (1992) suggests that the choice of bandwidth is more important than the choice of the type of kernel function. In this study, a triangular kernel is used for gaps due to its boundedness and a normal kernel is used for GVW. Detailed discussion on the kernel functions and bandwidths used are given elsewhere (OBrien and Enright 2011). In the simulation, kernel functions are used to modify the GVWs, gaps and speeds in a scenario each time it is selected. The modified GVW for a particular vehicle is then used to generate the number of axles for the vehicle based on the bivariate distribution of GVW and number of axles in the measured data. The axle spacings, and the weights carried out by each individual axle, are generated based on the measured distributions (Enright and OBrien 2012). Once all vehicles in a selected scenario have been generated, they are added to the simulated traffic stream, and the next scenario is then selected from the data. In this way, a continuous stream of simulated traffic is generated, and bridge load effects are calculated for this traffic using appropriate influence lines. Running the simulation for a sufficiently long time period substantially reduces the variance of the estimates of extreme loading (OBrien and Enright 2011).

For the simulated traffic scenarios, the bending moment load effect at each segment in the RC slab bridge is calculated. In an uncorrelated simulation, GVWs, slow-lane gaps and speeds are generated independently for each truck from the measured distribution in each lane.

Unlike the first, simpler example, the load model used in second example, accounts for the scenarios with trucks longer than 9m and trucks with more than three axles. It also accounts for a possibility of having more than one truck per lane on the bridge which will effectively add the same-lane gap correlation coefficient into the load model. Correlation between axle weights is also taken into account in scenario modelling. Figure 15 illustrates the bending moment distribution at segment no. 420 for correlated (grey dots) and uncorrelated (black dots) traffic models. Figure 15.a and Figure 15.b show bending moment distributions due to traffic load only and the combination of dead and traffic load respectively. The 75-year characteristic value is increased by 5% due to correlation in load effect distributions due to traffic load only. Taking account of self-weight results in a 1% increase in characteristic value which is 10 times greater than the increase in the first example due to 10% correlation coefficient of GVWs.

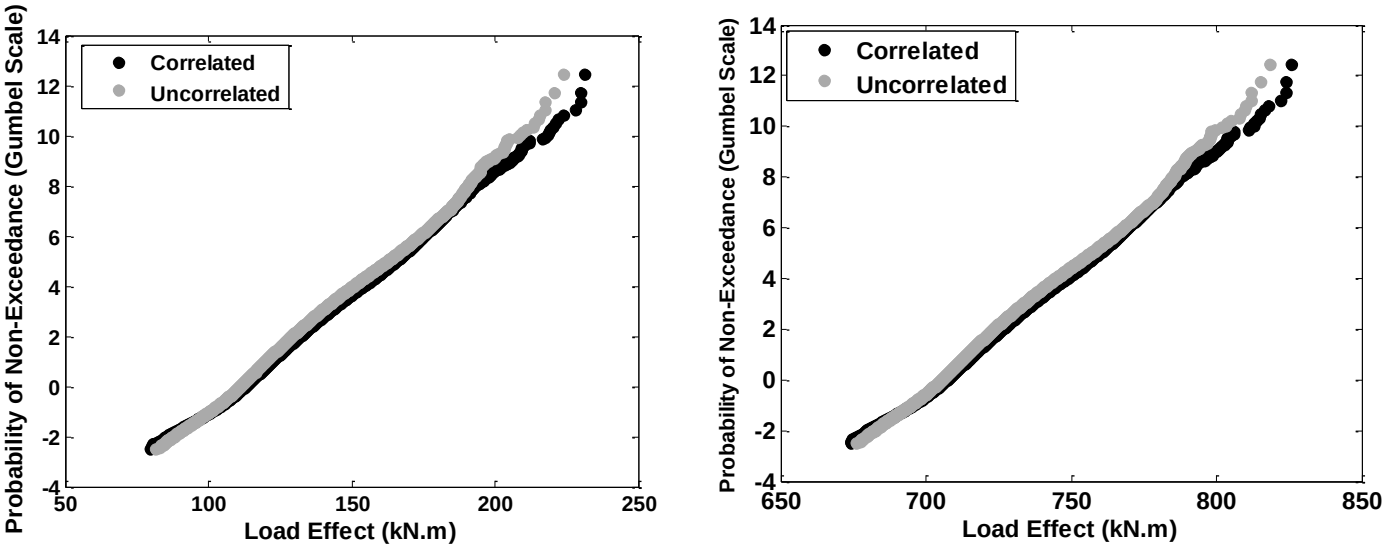

a. **Load effect due to live load** **b.** **Load effect due to dead and live load**

Figure 15 - Load effect distribution at segment no. 420

Figure 16.a illustrates the correlation coefficient pattern for segment nos. 401 to 440 for uncorrelated traffic scenarios. Figure 16.b is the corresponding correlation coefficients for correlated scenarios. It can be seen that the pattern and the magnitude do not change for correlated traffic.

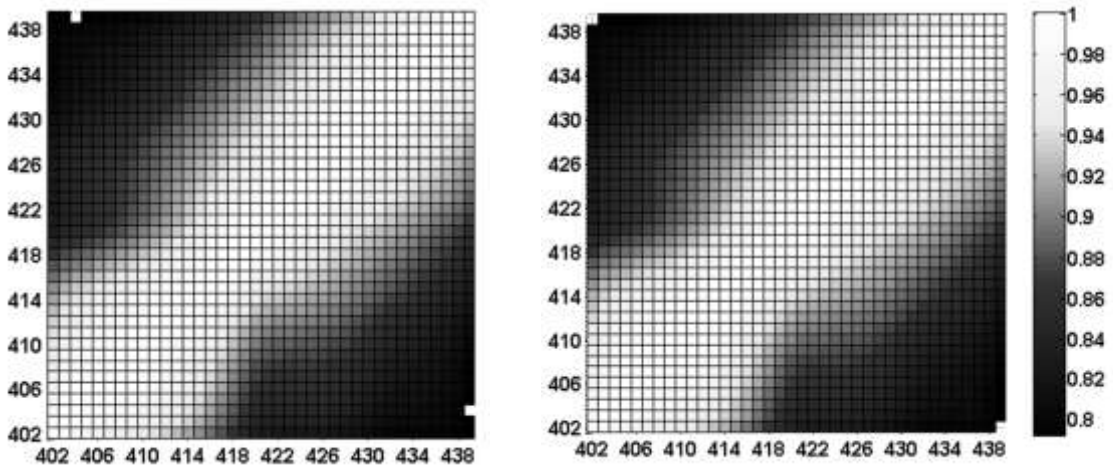

a. **Uncorrelated traffic** **b.** **Correlated traffic**

Figure 16 - correlation coefficient of load effects distribution for segments 401 to 440

Probability of failure

The same parameters given in Table 2 are used to generate the resistance distribution for this example and the same approach is used to calculate probability of failure using realistic traffic load. The progression of probability of failure with time is shown in Figure 17. This figure shows a similar trend to the probability of failure in the previous example. However, it can be seen that the realistic traffic model generally results in a lower probability of failure. The main reason is that the traffic measured in the Czech Republic is generally lighter than the traffic collected at the Netherlands.

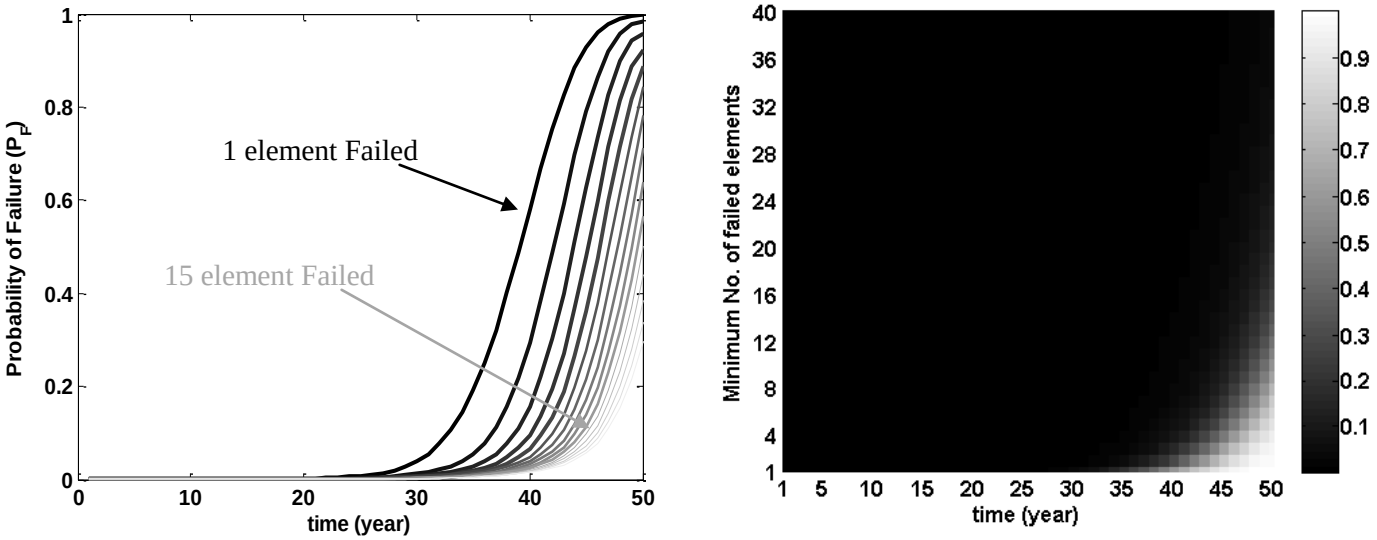

a. Probability of failure for different definitions **b. Contour plot**

Figure 17 - Probability of failure for correlated load and resistance

Probability of failure for different combinations of correlated and uncorrelated traffic and resistance are illustrated in Figure 18 for different definitions of probability of failure. It can be seen that the probability of correlated load and resistance is higher than uncorrelated load and resistance (approximately 2 times greater for 5^{th} and 6^{th} group). This figure also suggests that the increase in probability of failure is mainly due to the correlation of load scenarios rather than the correlation in resistance distributions. It is also shown that the increase in probability of failure due to correlation decreases by time. The comparison between these two example shows that the resistance correlation increases the probability of failure (almost 10% for the first year after corrosion); however the correlation of load model in the second example offers a greater increase in characteristic value which eventually results in a greater increase in probability of failure due to correlation of load.

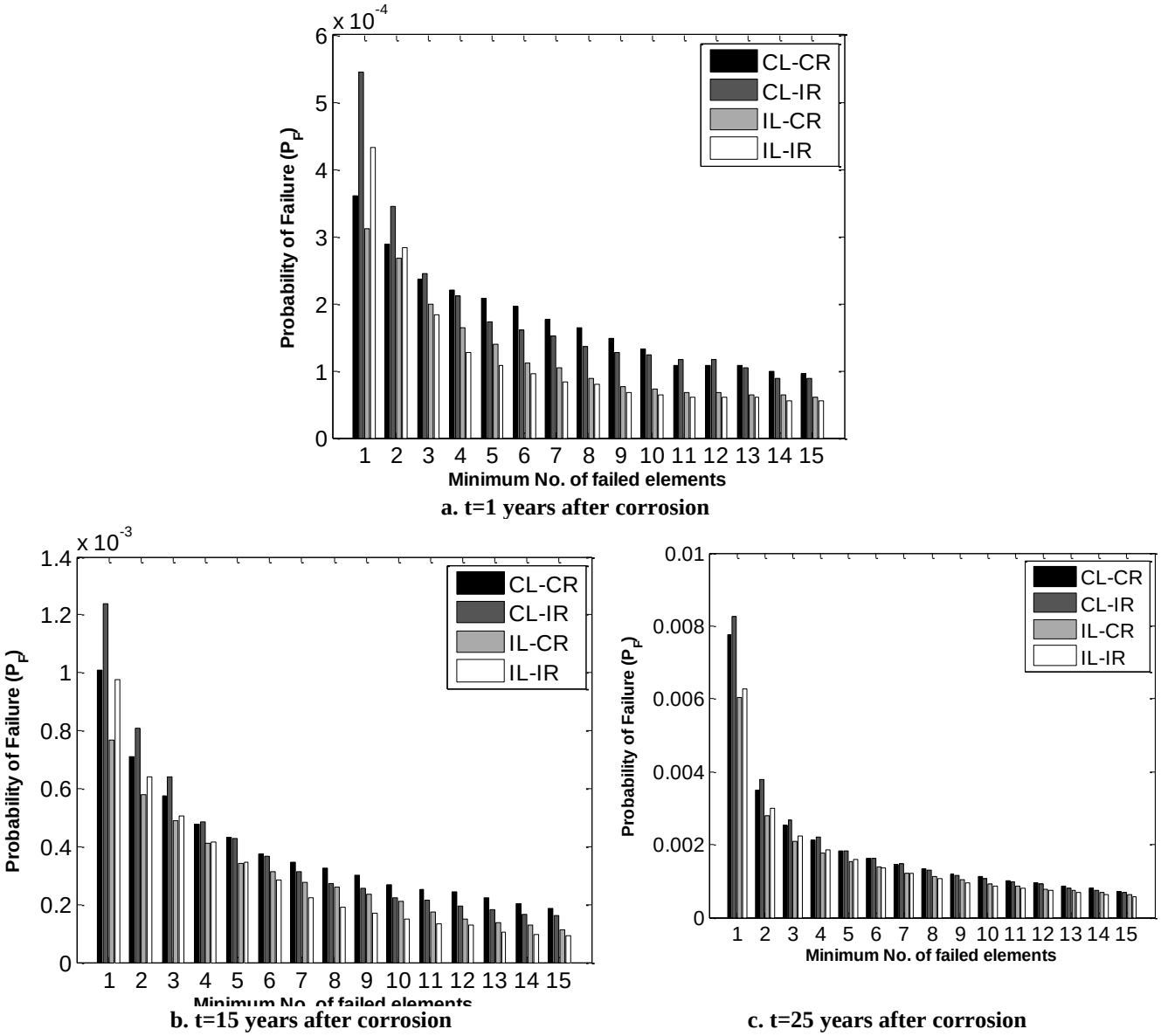

Figure 18- Probability of failure for correlated and uncorrelated traffic scenarios

7 Summary and Conclusion

There is evidence that resistance in reinforced concrete is correlated in time and space, and this becomes particularly apparent when modelling corrosion damage in RC structures. The effects of load are also spatially correlated, very strongly in this case, as the same vehicle passes over various segments of the bridge. This paper assesses the influence of resistance and load correlation on the time-dependent failure probability of a typical two-lane RC slab bridge under realistic traffic loading. A 2D random field model of the slab bridge is developed where concrete properties and cover are modelled as spatial variables. Random variables include pit depth and flexural model error. The effect of pitting corrosion and consequent loss of reinforcement cross-sectional area is considered through a time-dependent resistance model. Correlation of truck weights between trucks in adjacent lanes and inter-vehicle gap are also included and are calibrated against extensive WIM data. A 2D random field

is developed where time-dependent structural resistance and load effect are estimated for each segment in the random field.

It can be concluded from the results that the probability of failure depends on both load and resistance correlation but the effect is generally small. The effect of correlation on probability of failure is found to be also a function of time and failure definition. As the number of required failed elements increases and the time increases, the effect reduces.

8 Acknowledgement

This work is supported under the TEAM project. TEAM is a Marie Curie Initial Training Network and is funded by the European Commission 7th Framework Programme (PITN-GA-209-238648). The authors acknowledge the Dutch Ministry of Transport and Infrastructure, Rijkswaterstaat, for use of WIM data.

9 Reference

AASHTO. (2012). Bridge Design Specifications, American Association of State Highway and Transportation Officials, Washington DC, United States of America.

Akgül, F. and Frangopol, D. M. (2004a). Lifetime Performance Analysis of Existing Prestressed Concrete Bridge Superstructures. Journal of Structural Engineering, 130(12), 1889-1903.

Akgül, F. and Frangopol, D. M. (2004b). Time-Dependent Interaction between Load Rating and Reliability of Deteriorating Bridges. Engineering Structures, 26(12), 1751-1765.

Akiyama, M., Frangopol, D. M. and Yoshida, I. (2010). Time-Dependent Reliability Analysis of Existing Reinforced Concrete Structures in a Marine Environment Using Hazard Associated with Airborne Chlorides. Engineering Structures, 32(11), 3768-3779.

Ang, A. H. S. and Tang, W. H. (2007). Probability Concepts in Engineering Planning and Design - Basic Principles. Unites States of America, John Wiley & Sons Inc.

Attard, M. M. and Stewart, M. G. (1998). A Two Parameter Stress Block for High-Strength Concrete. ACI Structural Journal, 95(3), 305-317.

Bruls, A., Croce, P., Sanpaolesi, L. and Sedlacek, G. (1996). ENV1991–Part 3: Traffic Loads on Bridges; Calibration of Load Models for Road Bridges. Proceedings of IABSE Colloquium, Delft, Netherlands.

Castillo, E. (1988). Extreme Value Theory in Engineering (Statistical Modeling and Decision Science). Boston, United States of America, Academic Press.

Coronelli, D. and Gambarova, P. (2004). Structural Assessment of Corroded Reinforced Concrete Beams: Modeling Guidelines. Journal of Structural Engineering, 130(8), 1214-1224.

Costa, A. and Appleton, J. (1999). Chloride Penetration into Concrete in Marine Environment-Part II: Prediction of Long Term Chloride Penetration. Materials and Structures, 32(5), 354-359.

Darmawan, M. S. and Stewart, M. G. (2007). Spatial Time-Dependent Reliability Analysis of Corroding Pretensioned Prestressed Concrete Bridge Girders. Structural Safety, 29(1), 16-31.

Dawe, P. (2003). Research Perspectives: Traffic Loading on Highway Bridges. London, United Kingdom, Thomas Telford.

Der Kiureghian, A. and Ke, J.-B. (1988). The Stochastic Finite Element Method in Structural Reliability. Probabilistic Engineering Mechanics, 3(2), 83-91.

Du, Y. G., Clark, L. A. and Chan, A. H. C. (2005). Residual Capacity of Corroded Reinforcing Bars. Magazine of Concrete Research, 57(3), 135-147.

EC1. (2003). Actions on Structures-Part 2: Traffic Loads on Bridges, Eurocode1, EN1991-2:2003, European Committee for Standarization, Brussels.

Efron, B. and Tibshirani, R. J. (1994). An Introduction to the Bootstrap London, United Kingdom, Chapman & Hall/CRC Monographs on Statistics & Applied Probability.

Engelund, S. and Sørensen, J. D. (1998). A Probabilistic Model for Chloride-Ingress and Initiation of Corrosion in Reinforced Concrete Structures. Structural Safety, 20(1), 69-89.

Enright, B. (2010). Simulation of Traffic Loading on Highway Bridges. PhD Thesis, University College Dublin, Dublin, Ireland.

Enright, B. and OBrien, E. J. (2012). Monte Carlo Simulation of Extreme Traffic Loading on Short and Medium Span Bridges. Structure and Infrastructure Engineering, 1-16.

Fazio, R., Mirza, M., Cafferty, E. M., Andrews, R., Basheer, P. and Long, A. (1999). 26 IN-Situ Assessment of Corrosion-Induced Damage of the Dickson Bridge Deck. Durability of Building Materials and Components 8: Service Life and Durability of Materials and Components, 1, 269.

Frangopol, D. M., Kong, J. S. and Gharaibeh, E. S. (2001). Reliability-based Life-Cycle Management of Highway Bridges. Journal of Computing in Civil Engineering, 15(1), 27-34.

Gindy, M. and Nassif, H. H. (2006). Comparison of Traffic Load Models Based on Simulation and Measured Data. Joint International Conference on Coputing and Decision Making in Civil and Building Engineering, Montreal, Canada.

Haldar, A. and Mahadevan, S. (2000). Reliability Assessment Using Stochastic Finite Element Analysis. Unites States of America, John Wiley & Sons Inc.

Karimi, A., Ramachandran, K., Buenfeld, N. and Crowder, M. (2005). Probabilistic Analysis of Reinforcement Corrosion with Spatial Variability. Ninth International Conference on Structural Safety and Reliability, ICOSSAR 05, Rotterdam, Netherlands.

Kenshel, O. (2009). Influence of Spatial Variability on Whole Life Management of Reinforced Concrete Bridges. Ph.D Thesis, Trinity College Dublin, Dublin.

Kenshel, O. and O'Connor, A. J. (2009). Assessing Chloride-Induced Deterioration in Condition and Safety of Concrete Structures in Marine Environments. European Journal of Environmental and Civil Engineering, 13(5), 593-613.

Kersner, Z., Novák, D., Teply, B. and Rusina, R. (1998). Modeling of Deterioration of Concrete Structures by Stochastic Finite Element Method. Seventhth Intenational Conference on Structural Safety and Reliability, ICOSSAR 97, Kyoto, Japan, A. A. Balkema.

Kulicki, J. M., Prucz, Z., Clancy, C. M., Mertz, D. R. and Nowak, A. S. (2007). Updating the Calibration Report for AASHTO-LRFD code. Final Report for National Cooperative Highway Research Program (NCHRP). Washington DC, United States of America, Transportation Research Board.

Li, C.-C. and Der Kiureghian, A. (1993). Optimal Discretization of Random Fields. Journal of Engineering Mechanics, 119(6), 1136-1154.

Li, Y. (2004). Effect of Spatial Variability on Maintenance and Repair Decisions for Concrete Structures. PhD Thesis, TU Delpth, Delfth University of Technology, Delfth, Netherlands.

Li, Y., Vrouwenvelder, T., Wijnants, G. and Walraven, J. (2004). Spatial Variability of Concrete Deterioration and Repair Strategies. Structural Concrete, 5(3), 121-129.

Malioka, V. and Faber, M. H. (2004). Modeling of the Spatial Variability for Concrete Structures. Bridge Maintenance, Safety, Management and Cost - IABMAS 04, Rotterdam, Netherland, A. A. Balkema.

Mangat, P. S. and Elgarf, M. S. (1999). Flexural Strength of Concrete Beams with Corroding Reinforcement. ACI Structural Journal, 96(1).

Marsh, P. S. and Frangopol, D. M. (2008). Reinforced Concrete Bridge Deck Reliability Model Incorporating Temporal and Spatial Variations of Probabilistic Corrosion Rate Sensor Data. Reliability Engineering & System Safety, 93(3), 394-409.

Matthies, H. G., Brenner, C. E., Bucher, C. G. and Guedes Soares, C. (1997). Uncertainties in Probabilistic Numerical Analysis of Structures and Solids-Stochastic Finite Elements. Structural Safety, 19(3), 283-336.

Melchers, R. E. (1999). Structural Reliability: Analysis and Prediction. Unites States of America, John Wiley & Sons Inc.

Mori, Y. and Ellingwood, B. R. (1993). Reliability-based Service-Life Assessment of Aging Concrete Structures. Journal of Structural Engineering, 119(5), 1600-1621.

Mori, Y. and Ellingwood, B. R. (1994). Maintaining Reliability of Concrete Structures-I: Role of Inspection/Repair. Journal of Structural Engineering, 120(3), 824-845.

Nowak, A. S. (1993). Live Load Model for Highway Bridges. Structural Safety, 13(1-2), 53-66.
O'Connor, A. J. and Enevoldsen, I. (2007). Probability-based Assessment of an Existing Prestressed Post-Tensioned Concrete Bridge. Engineering Structures, 30, 1408-1416.
O'Connor, A. J., Pedersen, C., Gustavsson, L. and Enevoldsen, I. B. (2009). Probability-based Assessment and Optimised Maintenance Management of a Large Riveted Truss Railway Bridge. Structural Engineering International, 19(4), 375-382.
O'Connor, A. J. and Enevoldsen, I. (2009). Probability-based Assessment of Highway Bridges According to the New Danish Guideline. Structure and Infrastructure Engineering, 5(2), 157-168.
O'Connor, A. J., Jacob, B., OBrien, E. J. and Prat, M. (2001). Report of Current Studies Performed on Normal Load Model of EC1 Part 2: Traffic Loads on Bridges. Revue Française de Génie Civil, 5(4), 411-433.
O'Connor, A. J. and Kenshel, O. (2012). Experimental Evaluation of the Scale of Fluctuation for Spatial Variability Modeling of Chloride-Induced Reinforced Concrete Corrosion. Journal of Bridge Engineering, 18(1), 3-14.
OBrien, E. J. and Enright, B. (2011). Modeling Same-Direction Two-Lane Traffic for Bridge Loading. Structural Safety, 33(4-5), 296-304.
Rodriguez, J., Ortega, L. M. and Casal, J. (1997). Load Carrying Capacity of Concrete Structures with Corroded Reinforcement. Construction and Building Materials, 11(4), 239-248.
Scott, D. W. (1992). Multivariate Density Estimation: Theory, Practice, and Visualization. New York, United States of America, John Wiley & Sons Inc.
Sheikh, A. K., Boah, J. K. and Hansen, D. A. (1990). Statistical Modeling of Pitting Corrosion and Pipeline Reliability. Corrosion, The Journal of Science and Engineering, 46(3), 190-197.
Sterritt, G., Chryssanthopoulos, M. K. and Shetty, N. (2001). Reliability-based Inspection Planning for RC Highway Bridges. Safety, Risk and Reliability-Trends in Engineering, Zurich, Switzerland, International Association for Bridge and Structural Engineering.
Stewart, M. G. (1995). Workmanship and Its Influence on Probabilistic Models of Concrete Compressive Strength. ACI Materials Journal, 92(4), 361-372.
Stewart, M. G. (2004). Spatial Variability of Pitting Corrosion and its Influence on Structural Fragility and Reliability of RC Beams in Flexure. Structural Safety, 26(4), 453-470.
Stewart, M. G. (2005). Life-Cycle Cost analysis Considering Spatial and Temporal Variability of Corrosion-Induced Damage and Repair to Concrete Surface. International Conference on Structural Safety and Reliability, ICOSSAR 05.
Stewart, M. G. (2006). Spatial Variability of Damage and Expected Maintenance Costs for Deteriorating RC Structures. Structure & Infrastructure Engineering, 2(2), 79-90.
Stewart, M. G. (2009). Mechanical Behaviour of Pitting Corrosion of Flexural and Shear Reinforcement and its Effect on Structural Reliability of Corroding RC Beams. Structural Safety, 31(1), 19-30.
Stewart, M. G. and Al-Harthy, A. (2008). Pitting Corrosion and Structural Reliability of Corroding RC Structures: Experimental Data and Probabilistic Analysis. Reliability Engineering & System Safety, 93(3), 373-382.
Stewart, M. G. and Mullard, J. A. (2007). Spatial Time-Dependent Reliability Analysis of Corrosion Damage and the Timing of First Repair for RC Structures. Engineering Structures, 29(7), 1457-1464.
Stewart, M. G. and Rosowsky, D. V. (1998). Structural Safety and Serviceability of Concrete Bridges Subject to Corrosion. Journal of Infrastructure Systems, 4(4), 146-155.
Stewart, M. G. and Suo, Q. (2009). Extent of Spatially Variable Corrosion Damage as an Indicator of Strength and Time-Dependent Reliability of RC Beams. Engineering Structures, 31(1), 198-207.
Stewart, M. G. and Val, D. V. (2003). Multiple Limit States and Expected Failure Costs for Deteriorating Reinforced Concrete Bridges. Journal of Bridge Engineering, 8(6), 405-415.
Sudret, B., Defaux, G. and Pendola, M. (2006). Introducing Spatial Variability in the Lifetime Assessment of a Concrete Beam Submitted to Rebar's Corrosion. Proceeding of 2nd International Forum on Engineering Decision Making, Lake Louise, Canada.

Sudret, B., Defaux, G. and Pendola, M. (2007). Stochastic Evaluation of the Damage Length in RC Beams Submitted to Corrosion of Reinforcing Steel. Civil Engineering and Environmental Systems, 24(2), 165-178.

Sudret, B. and Der Kiureghian, A. (2000). Stochastic Finite Element Methods and Reliability: a State-of-the-Art Report. California, United States of America, Department of Civil and Environmental Engineering, University of California.

Torres-Acosta, A. A. and Martinez-Madrid, M. (2003). Residual Life of Corroding Reinforced Concrete Structures in Marine Environment. Journal of Materials in Civil Engineering, 15(4), 344-353.

Val, D. V. and Melchers, R. E. (1997). Reliability of Deteriorating RC Slab Bridges. Journal of Structural Engineering, 123(12), 1638-1644.

Val, D. V., Stewart, M. G. and Melchers, R. E. (2000). Life-Cycle Performance of RC Bridges: Probabilistic Approach. Computer-Aided Civil and Infrastructure Engineering, 15(1), 14-25.

Van Daveer, J. R. (1975). Techniques for Evaluating Reinforced Concrete Bridge Decks. Journal of American Concrete Institute, 72(12), 697-704.

Vanmarcke, E. (1985). Random Fields: Analysis and Synthesis. London, United Kingdom, MIT Press.

Vu, K. A. and Stewart, M. G. (2005). Predicting the Likelihood and Extent of Reinforced Concrete Corrosion-Induced Cracking. Journal of Structural Engineering, 131(11), 1681-1689.

Vu, K. A. T. (2003). Corrosion-Induced Cracking and Spatial Time-Dependant Reliability Analysis of Reinforced Concrete Structures. PhD Thesis, The University of Newcastle, Newcastle, Australia.

Vu, K. A. T. and Stewart, M. G. (2000). Structural Reliability of Concrete Bridges Including Improved Chloride-Induced Corrosion Models. Structural Safety, 22(4), 313-333.

Zhai, X. and Stewart, M. G. (2010). Structural Reliability Analysis of Reinforced Grouted Concrete Block Masonry Walls in Compression. Engineering Structures, 32(1), 106-114.